Research Article

Yun-Jie Xu, Sohail A. Khan, Muhammad Ijaz Khan*, Faris Alzahrani, and Omar T. Bafakeeh

Irreversibility analysis in time-dependent Darcy–Forchheimer flow of viscous fluid with diffusion-thermo and thermo-diffusion effects

https://doi.org/10.1515/phys-2022-0136
received February 25, 2021; accepted March 21, 2022

Abstract: In this article, we analyze the entropy analysis in unsteady hydromagnetic flow of a viscous fluid over a stretching surface. The energy attribute is scrutinized through dissipation, heat source/sink, and radiation. Furthermore, diffusion-thermo and thermo-diffusion behaviors are analyzed. The physical description of the entropy rate is discussed through the second law of thermodynamics. Additionally, a binary chemical reaction is considered. Partial differential equations are transformed into ordinary ones by adequate variables. Here, we used an optimal homotopy analysis method (OHAM) to develop a convergent solution. The influence of flow variables on velocity, Bejan number, thermal field, concentration, and entropy rate is examined through graphs. The physical performance of drag force, Sherwood number, and temperature gradient *versus* influential variables is studied. A similar effect holds for velocity through variation of porosity and magnetic variables. An increment in thermal field and entropy rate is noted through radiation. A reverse trend holds for the Bejan number and thermal field through a magnetic variable. An augmentation in the Soret number enhances the concentration. An amplification in drag force is noted through the Forchheimer number. Higher estimation of radiation corresponds to a rise in the heat transfer rate.

Keywords: Darcy–Forchheimer model, entropy generation, viscous dissipation, heat source/sink, chemical reaction, thermal radiation and Soret and Dufour effects

Nomenclature

ρ	density
μ	dynamic viscosity
σ	electrical conductivity
ν	kinematic viscosity
λ	porosity variable
γ	reaction variable
α_1	temperature difference variable
α_2	concentration difference variable
τ_w	shear stress
A	unsteady variable
Be	Bejan number
Br	Brinkman number
C	concentration
C_∞	ambient concentration
C_b	drag force
C_{fx}	drag force
C_s	concentration susceptibility
C_w	wall concentration
Du	Dufour number
Ec	Eckert number
F	inertia coefficient
Fr	Forchheimer number
g	gravitational acceleration
j_w	mass flux
K	porous medium permeability
k_r	reaction rate
K_T	thermal diffusion ratio
L	diffusion variable
k^*	mean absorption coefficient

* **Corresponding author: Muhammad Ijaz Khan,** Department of Mathematics and Statistics, Riphah International University, I-14, Islamabad 44000, Pakistan; Nonlinear Analysis and Applied Mathematics (NAAM)-Research Group, Department of Mathematics, Faculty of Sciences, King Abdulaziz University, P.O. Box 80203, Jeddah, 21589, Saudi Arabia, e-mail: mikhan@math.qau.edu.pk
Yun-Jie Xu: School of Engineering, Huzhou University, Huzhou 313000, China
Sohail A. Khan: Department of Mathematics, Quaid-I-Azam University 45320, Islamabad 44000, Pakistan
Faris Alzahrani: Mathematical Modeling and Applied Computation (MMAC) Research Group, Department of Mathematics, King Abdulaziz University, Jeddah 21589, Saudi Arabia
Omar T. Bafakeeh: Department of Industrial Engineering, Jazan University, Jazan 82822, Saudi Arabia

N_G	entropy rate
Nu_x	Nusselt number
Pr	Prandtl number
q_w	heat flux
Rd	radiation variable
Sc	Schmidt number
Sh_x	Sherwood number
Sr	Soret number
σ^*	Stephan–Boltzman constant
T	temperature
T_∞	ambient temperature
T_m	mean fluid temperature
T_w	wall temperature
u, v	velocity components
x, y	Cartesian coordinates

1 Introduction

The Dufour effect (thermo-diffusion) is the mechanism in which heat transfer occurs under a concentration gradient (mass). In contrast, the Soret effect (diffusion-thermo) is the process in which solutal transfer occurs under a temperature gradient. Thermo-diffusion and diffusion-thermo play a substantial role when there is high density difference in the liquid flow region. These effects are effective in combined solutal and thermal transport in the binary system for transitional nuclear weight gases. Consequently, in the modern area, various engineers, scientists, and researchers have concentrated their attention on Dufour (thermo-diffusion) and Soret (diffusion-thermo) effect problems because of their widespread applications in different fields such as nuclear waste repositories, drag reduction, energy storage units, heat insulation, plasma actuators, catalytic reactors, geothermal systems, energy systems, drying technology, and many others. The heat transfer effect in hydromagnetic non-Darcian convective flow of a viscous liquid subjected to a porous medium with thermo-diffusion and diffusion-thermo effects was discussed by Mahdy [1]. The unsteady hydromagnetic flow of viscous liquid with Soret and Dufour effects toward a stretchable surface was discussed by Raveendra *et al.* [2]. Khan *et al.* [3] conducted the entropy analysis of viscous liquid flow with Dufour and Soret effects over a rotating cone. Reddy and Chamkha [4] studied the variable heat source/sink in time-dependent viscous liquid flow subjected to a permeable surface with diffusion-thermo and diffusion-thermo effects. Also, useful studies in this field can be found in refs. [5–13].

Radiation has a considerable impact on the heat transit phenomenon in electrically driven flows over any surface. Radiation is regarded as a decisive parameter in controlling the heat transfer rate used by processes involving high temperatures. On the other hand, because of its comprehensive applications, the Joule heating effect, which occurs due to interactions between fluid particles, has maintained prominence. Due to its resistive heating property, Joule heating is utilized in nuclear engineering, electrical appliances, iron soldering, glycol vaporizing, and many more applications. In the manufacturing industry, the flow of radiation heat transfer is critical for the design of reliable machinery, gas turbines, nuclear power plants, and a variety of propulsion technologies, such as, satellites, aircraft, and space vehicles. Mahanthesh *et al.* [14] worked on radiation analysis of a hybrid Al_2O_3–H_2O nanoliquid by a vertical plate. The forced convective hydromagnetic flow of hybrid nanomaterials with the radiation effect was illuminated by Sulochana *et al.* [15]. Numerous researchers [16–30] elaborated, in their studies, on the significance of radiation and its effect on fluid flow.

Nowadays, the essential concern of engineers and researchers is to determine the mechanism that can manage the consumption of good energy. It is a well-known fact that all thermal devices work on the thermodynamics principle and produce an irreversibility phenomenon. Entropy minimization is necessary to enhance efficiency of thermodynamical systems such as refrigerators, power plants, thermal storage devices, environmental control of aircraft, heat exchanger design, and electronic device cooling systems. Irreversibility analysis problems have gained more consideration due to astonishing applications in power collectors, fuel cells, slider bearings, geothermal processes, engineering phenomena, geothermal energy systems, and advanced nanotechnology. Entropy generation occurs through the Joule–Thomson effect, fluid friction, thermal flux, Joule heating, molecular vibration, mass flux, radiation, and many other effects. Bejan [31,32] discussed theoretical work on entropy problems in fluid flow with thermal transportation. Khan *et al.* [33] performed the entropy and melting analysis for the hydromagnetic flow of nanoliquid with radiation over a stretchable surface. Irreversibility analysis of the Darcy–Forchheimer flow of CNT-based nanomaterials with Lorentz force over a porous surface was studied by Seth *et al.* [34]. Entropy analysis of the hydromagnetic flow of a power-law fluid with Dufour and Soret behaviors in a permeable cavity was highlighted by Kefayati [35]. Some important studies in this field are highlighted in refs. [35–45].

The above-mentioned evaluations indicate that no effort has been made to investigate the effect of entropy on time-dependent Darcy–Forchheimer flow of a viscous fluid with Lorentz force over a permeable surface. Yet, in recent times, numerous researchers have scrutinized the Soret and Dufour effects in viscous liquid with entropy rate over a permeable surface. Here, the prime objective of this work is to address the aspects of irreversibility analysis of Darcy–Forchheimer flow of a viscous fluid over a stretching permeable surface. Heat communication is discussed with dissipation heat source/sink and radiation. Furthermore, Soret and Dufour behaviors are also addressed. The physical description of irreversibility analysis is given. The first-order reaction is considered. Ordinary differential systems are obtained through adequate variables. Here, we used the optimal homotopy analysis method (OHAM) to construct a convergent solution [46,47]. Significant impacts of sundry variables on entropy rate, velocity field, thermal field, Bejan number, and concentration are graphically discussed. The influence of flow variables on drag force, concentration gradient and Nusselt number are studied. A comparison study with published studies is highlighted in Table 1, which shows an excellent agreement.

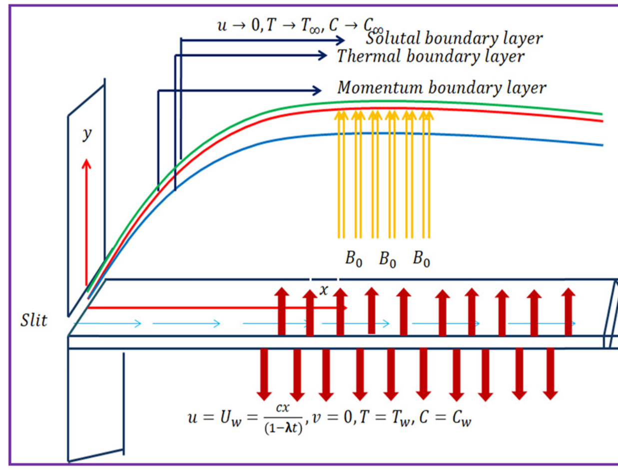

Figure 1: Flow diagram.

2 Methodology

Consider time-dependent hydromagnetic Darcy–Forchheimer flow of a viscous fluid over a permeable surface. Dissipation, heat source/sink, and radiation are considered in the heat expression. Thermo-diffusion and diffusion-thermo effects are also addressed. The physical feature of entropy analysis is discussed through the second law of thermodynamics. The first-order reaction rate is also taken into account. The magnetic force of strength (B_0) is incorporated. Let us suppose that $u\left(=u_w = \frac{cx}{(1-\lambda t)}\right)$ is the stretching velocity with a positive rate constant. The induced magnetic field is neglected due to the low magnetic Reynolds number. The flow sketch is highlighted in Figure 1.

Table 1: Comparative results of heat transfer rate with [46,47]

Pr	Wang [46]	Gorla and Sidawi [47]	Current result
0.07	0.0656	0.0656	0.0655
0.20	0.1691	0.1691	0.1692
0.70	0.4539	0.4539	0.4540
2.00	0.9114	0.9114	0.9115
7.00	1.8954	1.8954	1.8953
20.00	3.3539	3.3539	3.3538
70.00	6.4622	6.4622	6.4623

The governing equation satisfies

$$\frac{\partial u}{\partial x} + \frac{\partial v}{\partial y} = 0, \tag{1}$$

$$\frac{\partial u}{\partial t} + u\frac{\partial u}{\partial x} + v\frac{\partial u}{\partial y} = \nu\frac{\partial^2 u}{\partial y^2} - \frac{\sigma B_0^2}{\rho}u - \frac{\nu}{K}u - \mathrm{F}u^2, \tag{2}$$

$$\begin{aligned}\frac{\partial T}{\partial t} + u\frac{\partial T}{\partial x} + v\frac{\partial T}{\partial y} &= \alpha\frac{\partial^2 T}{\partial y^2} + \frac{D_m K_T}{C_s c_p}\frac{\partial^2 C}{\partial y^2} \\ &+ \frac{\mu}{(\rho c_p)}\left(\frac{\partial u}{\partial y}\right)^2 + \frac{16}{3}\frac{\sigma^* T_\infty^3}{k^*(\rho c_p)}\frac{\partial^2 T}{\partial y^2} \\ &+ \frac{Q_0}{(\rho c_p)}(T - T_\infty),\end{aligned} \tag{3}$$

$$\begin{aligned}\frac{\partial C}{\partial t} + u\frac{\partial C}{\partial x} + v\frac{\partial C}{\partial y} &= D_m\frac{\partial^2 C}{\partial y^2} + \frac{D_m k_T}{T_m}\frac{\partial^2 T}{\partial y^2} \\ &- k_r(C - C_\infty).\end{aligned} \tag{4}$$

For $t > 0$, we have

$$\left.\begin{array}{l} u = u_w,\ \ v = 0,\ \ T = T_w,\ \ C = C_w \quad \text{at } y = 0 \\ u \to 0,\ \ T = T_\infty,\ \ C = C_\infty \quad \text{when } y \to \infty \end{array}\right\}. \tag{5}$$

Considering

$$\left.\begin{array}{l} u = \frac{cx}{(1-\lambda t)}f'(\eta),\ \ v = -\sqrt{\frac{c\nu}{(1-\lambda t)}}f(\eta), \\ T = T_\infty + T_w\left[\frac{cx}{2\nu(1-\lambda t)^2}\right]\theta(\eta), \\ C = C_\infty + C_w\left[\frac{cx}{2\nu(1-\lambda t)^2}\right]\phi(\eta),\ \ \eta = \sqrt{\frac{\nu}{\nu(1-\lambda t)}}y \end{array}\right\}, \tag{6}$$

one obtains

$$f''' + ff'' - f'^2 - \frac{A}{2}\eta f'' - (M + A + \lambda)f' - Frf'^2 = 0, \tag{7}$$

$$(1+\mathrm{Rd})\theta'' + \Pr f\theta' - \Pr f'\theta - \frac{A}{2}\Pr \eta\theta' - 2\Pr A\theta + \Pr \mathrm{Du}\phi'' + \Pr \mathrm{Ec}f''^2 + \Pr Q\theta = 0, \quad (8)$$

$$\phi'' + \mathrm{Sc}f\phi' - \mathrm{Sc}f'\phi - \frac{A}{2}\mathrm{Sc}\eta\phi' - 2\mathrm{Sc}A\phi + \mathrm{Sc}\mathrm{Sr}\theta'' - \gamma\mathrm{Sc}\phi = 0, \quad (9)$$

$$\left.\begin{array}{l} f(0)=0,\; f'(0)=1,\; \theta(0)=1,\; \phi(0)=1 \\ f'(\infty)=0,\; \theta(\infty)=0,\; \phi(\infty)=0 \end{array}\right\}. \quad (10)$$

Here, dimensionless variables are $A\left(=\frac{\lambda}{c}\right)$, $\lambda\left(=\frac{\nu(1-\lambda t)}{Kc}\right)$, $M\left(=\frac{\sigma B_0^2(1-\lambda t)}{c\rho}\right)$, $D_f\left(=\frac{D_m K_T C_w}{\nu C_s c_p T_w}\right)$, $\Pr\left(=\frac{\nu}{\alpha}\right)$, $\mathrm{Fr}\left(=\frac{C_b x}{K^{1/2}}\right)$, $\mathrm{Ec}\left(=\frac{2\nu cx}{T_w c_p}\right)$, $\mathrm{Br}(=\Pr\,\mathrm{Ec})$, $\mathrm{Rd}\left(=\frac{16}{3}\frac{\sigma^* T_\infty^3}{k^* k}\right)$, $\mathrm{Sc}\left(=\frac{\nu}{D_m}\right)$, $\lambda\left(=\frac{k_r(1-\lambda t)}{c}\right)$, and $\mathrm{Sr}\left(=\frac{D_m K_T T_w}{\nu C_w T_m}\right)$.

2.1 Entropy generation

Entropy generation is defined as [33–39]

$$\left.\begin{array}{l} S_G = \frac{k}{T_\infty^2}\left(1+\frac{16}{3}\frac{\sigma^* T_\infty^3}{k^* k}\right)\left(\frac{\partial T}{\partial y}\right)^2 + \frac{\mu}{T_\infty}\left(\frac{\partial u}{\partial y}\right)^2 + \frac{\mu}{KT_\infty}u^2 \\ + \frac{R_D}{T_\infty}\left(\frac{\partial T}{\partial y}\frac{\partial C}{\partial y}\right) + \frac{R_D}{C_\infty}\left(\frac{\partial C}{\partial y}\right)^2 \end{array}\right\}, \quad (11)$$

One can find

$$N_G = \alpha_1 \mathrm{Re}(1+\mathrm{Rd})\,\theta'^2 + \frac{1}{2}\mathrm{Br}f''^2 + \frac{1}{2}\lambda \mathrm{Br}f'^2 + L\,\mathrm{Re}\theta'\phi' + L\,\mathrm{Re}\frac{\alpha_2}{\alpha_1}\phi'^2. \quad (12)$$

The Bejan number (Be) is mathematically written as follows:

$$\mathrm{Be} = \frac{\text{Heat and mass transfer irreversibility}}{\text{Total irreversibility}}, \quad (13)$$

or

$$\mathrm{Be} = \frac{N_G = \alpha_1\mathrm{Re}(1+\mathrm{Rd})\,\theta'^2 + L\,\mathrm{Re}\theta'\phi' + L\,\mathrm{Re}\frac{\alpha_2}{\alpha_1}\phi'^2}{N_G = \alpha_1\mathrm{Re}(1+\mathrm{Rd})\theta'^2 + \frac{1}{2}\mathrm{Br}f''^2 + \frac{1}{2}\lambda\mathrm{Br}f'^2 + L\,\mathrm{Re}\theta'\phi' + L\,\mathrm{Re}\frac{\alpha_2}{\alpha_1}\phi'^2}. \quad (14)$$

in which dimensionless parameters are $N_G\left(=\frac{S_G \nu^2(1-\lambda t)^3 T_\infty}{kcxT_w}\right)$, $\alpha_1\left(=\frac{T_w}{T_\infty}\right)$, $\alpha_2\left(=\frac{C_w}{C_\infty}\right)$ and $L\left(=\frac{R_D(C_0-C_\infty)}{k}\right)$.

2.2 Quantities of interest

2.2.1 Surface drag force

Surface drag force is defined by

$$C_{fx} = \frac{\tau_w}{\rho u_w^2}, \quad (15)$$

τ_w shear stress satisfy

$$\tau_w = \mu\frac{\partial u}{\partial y}\bigg|_{y=0}. \quad (16)$$

We have

$$C_{fx}\mathrm{Re}_x^{\frac{1}{2}} = f''(0). \quad (17)$$

2.2.2 Heat transfer rate

Mathematically

$$\mathrm{Nu}_x = \left(\frac{2\nu}{c}\right)^2\frac{(1-\lambda t)}{kT_w}\left(\frac{2\nu}{c}\right)q_w, \quad (18)$$

and q_w heat flux is given by

$$q_w = -k\left(\frac{\partial T}{\partial z}\right) - \frac{16}{3}\frac{\sigma^* T_\infty^3}{k^*}\left(\frac{\partial T}{\partial y}\right), \quad (19)$$

one can find

$$\mathrm{Nu}_x\mathrm{Re}_x^{-1/2} = -(1+\mathrm{Rd})\theta'(0). \quad (20)$$

2.2.3 Mass transfer rate

Mathematically

$$\mathrm{Sh}_x = \left(\frac{2\nu}{c}\right)^2\frac{(1-\lambda t)}{D_m C_w}\left(\frac{2\nu}{c}\right)j_w, \quad (21)$$

and j_w mass flux is

$$j_w = -D_m\left(\frac{\partial C}{\partial y}\right) \quad (22)$$

or

$$\mathrm{Sh}_x\mathrm{Re}_x^{-1/2} = -\phi'(0). \quad (23)$$

2.3 Solutions

Linear operators and initial guesses for OHAM satisfy

$$\left.\begin{aligned} f_0(\eta) &= 1 - e^{-\eta},\\ \theta_0(\eta) &= e^{-\eta},\\ \phi_0(\eta) &= e^{-\eta}, \end{aligned}\right\}, \tag{24}$$

$$\left.\begin{aligned} L_f &= \frac{\partial^3}{\partial\eta^3} - \frac{\partial}{\partial\eta},\\ L_\theta &= \frac{\partial^2}{\partial\eta^2} - 1,\\ L_\phi &= \frac{\partial^2}{\partial\eta^2} - 1, \end{aligned}\right\}, \tag{25}$$

with

$$\left.\begin{aligned} &L_f = [a_0 + a_1e^{\eta} + a_2e^{-\eta}],\quad L_\theta = [a_3e^{\eta} + a_4e^{-\eta}],\\ &L_\phi = [a_5e^{\eta} + a_6e^{-\eta}], \end{aligned}\right\}, \tag{26}$$

here a_i (i = 0, 2, 3, ..., 6) signify the arbitrary constants.

Suppose that $\hbar_f$, $\hbar_\theta$, and $\hbar_\phi$ are auxiliary variables and $q \in [0, 1]$ the embedding variable.

2.3.1 Zeroth-order deformation problems

It is given by

$$(1 - p)\,\mathbf{L}_1[F(\eta; p) - f_0(\eta)] = p\hbar_f\mathfrak{R}_f\mathbf{L}_f[F(\eta; p)], \tag{27}$$

$$(1 - p)\,\mathbf{L}_2[\theta(\eta; p) - \theta_0(\eta)] = p\hbar_\theta\mathfrak{R}_\theta\mathbf{L}_\theta[\theta(\eta; p)], \tag{28}$$

$$(1 - p)\,\mathbf{L}_3[\phi(\eta; p) - \phi_0(\eta)] = p\hbar_\phi\mathfrak{R}_\phi\mathbf{L}_\phi[\phi(\eta; p)], \tag{29}$$

$$\left.\begin{aligned} &F'(0; p) = 1,\ F(0; p) = 0,\ F'(\infty; p) = 0,\\ &\theta(0; p) = 1,\\ &\theta(\infty; p) = 0,\ \phi(0; p) = 1,\ \phi(\infty; p) = 0. \end{aligned}\right\} \tag{30}$$

Linear operators are defined as

$$\left.\begin{aligned} \mathbf{L}_f = {} & \frac{\partial^3F(\eta; p)}{\partial\eta^3} + F(\eta; p)\,\frac{\partial^2F(\eta; p)}{\partial\eta^2} - \frac{A}{2}\eta\frac{\partial^2F(\eta; p)}{\partial\eta^2}\\ & - \left(\frac{\partial F(\eta; p)}{\partial\eta}\right)^2 - A\left(\frac{\partial F(\eta; p)}{\partial\eta}\right)\\ & - M\left(\frac{\partial F(\eta; p)}{\partial\eta}\right) - \lambda\left(\frac{\partial F(\eta; p)}{\partial\eta}\right) - \mathrm{Fr}\left(\frac{\partial F(\eta; p)}{\partial\eta}\right)^2, \end{aligned}\right\} \tag{31}$$

$$\left.\begin{aligned} \mathbf{L}_\theta = {} & \frac{\partial^2\theta(\eta; p)}{\partial\eta^2} + \mathrm{Rd}\frac{\partial^2\theta(\eta; p)}{\partial\eta^2} + \Pr\left(F(\eta; p)\,\frac{\partial\theta(\eta; p)}{\partial\eta}\right)\\ & - \Pr\left(\theta(\eta; p)\,\frac{\partial F(\eta; p)}{\partial\eta}\right) - \frac{A}{2}\Pr\eta\frac{\partial\theta(\eta; p)}{\partial\eta}\\ & - 2\Pr A\theta(\eta; p) + \Pr D_f\frac{\partial^2\varphi(\eta; p)}{\partial\eta^2} + \Pr\mathrm{Ec}\left(\frac{\partial^2F(\eta; p)}{\partial\eta^2}\right)^2\\ & + \Pr Q\theta(\eta; p), \end{aligned}\right\} \tag{32}$$

$$\left.\begin{aligned} \mathbf{L}_\phi = {} & \frac{\partial^2\phi(\eta; p)}{\partial\eta^2} + \mathrm{Sc}\left(F(\eta; p)\,\frac{\partial\phi(\eta; p)}{\partial\eta}\right)\\ & - \mathrm{Sc}\left(\phi(\eta; p)\,\frac{\partial F(\eta; p)}{\partial\eta}\right) - \frac{A}{2}\mathrm{Sc}\,\eta\frac{\partial\phi(\eta; p)}{\partial\eta}\\ & - 2\mathrm{Sc}\,A\phi(\eta; p)\\ & + \mathrm{Sc}S_r\frac{\partial^2\theta(\eta; p)}{\partial\eta^2} - \gamma\,\mathrm{Sc}\phi(\eta; p) \end{aligned}\right\}. \tag{33}$$

2.3.2 *M*-th order deformation problems

M-th order problems satisfy

$$\mathbf{L}_1[f_m - \chi_m f_{m-1}] = \hbar_f R_m^f, \tag{34}$$

$$\mathbf{L}_2[\theta_m - \chi_m\theta_{m-1}] = \hbar_\theta R_m^\theta, \tag{35}$$

$$\mathbf{L}_2[\phi_m - \chi_m\phi_{m-1}] = \hbar_\phi R_m^\phi, \tag{36}$$

$$\left.\begin{aligned} &\frac{\partial f_m}{\partial\eta}\bigg|_{\eta=0} = f_m|_{\eta=0} = \frac{\partial f_m}{\partial\eta}\bigg|_{\eta=\infty} = 0,\\ &\frac{\partial\theta_m}{\partial\eta}\bigg|_{\eta=0} = \theta_m|_{\eta=\infty} = 0,\\ &\frac{\partial\phi_m}{\partial\eta}\bigg|_{\eta=0} = \phi_m|_{\eta=\infty} = 0, \end{aligned}\right\} \tag{37}$$

$$\left.\begin{aligned} R_m^f = {} & f_{m-1}''' + \sum_{k=0}^{m-1} f_{m-1-k}f_k'' - \frac{A}{2}\eta f_{m-1}''\\ & - \sum_{k=0}^{m-1} f_{m-1-k}'f_k' - Mf_{m-1}' - Af_{m-1}' - \lambda f_{m-1}'\\ & - \mathrm{Fr}\sum_{k=0}^{m-1} f_{m-1-k}'f_k', \end{aligned}\right\} \tag{38}$$

$$\left.\begin{aligned} R_m^\theta = {} & (1+\mathrm{Rd})\,\theta_{m-1}'' + \Pr\sum_{k=0}^{m-1} f_{m-1-k}\theta_k'\\ & - \Pr\sum_{k=0}^{m-1}\theta_{m-1-k}f_k' - \frac{A}{2}\Pr\eta\theta_{m-1}' - 2\Pr A\theta_{m-1}\\ & + \Pr D_f\phi_{m-1}'' + \mathrm{Br}\sum_{k=0}^{m-1} f_{m-1-k}''f_k'' + \Pr Q\theta_{m-1}, \end{aligned}\right\} \tag{39}$$

$$\left.\begin{aligned} R_m^\phi = {} & \phi_{m-1}'' + \mathrm{Sc}\sum_{k=0}^{m-1} f_{m-1-k}\phi_k' - \mathrm{Sc}\sum_{k=0}^{m-1}\phi_{m-1-k}f_k'\\ & - \frac{A}{2}\mathrm{Sc}\,\eta\phi_{m-1}' - 2\mathrm{Sc}\,A\phi_{m-1}\\ & + \mathrm{Sc}\,S_r\theta_{m-1}'' - \gamma\mathrm{Sc}\phi_{m-1}. \end{aligned}\right\} \tag{40}$$

$$\chi_m = \begin{cases} 0, & m \le 1,\\ 1, & m > 1. \end{cases} \tag{41}$$

2.4 Convergence analysis

Initially, Liao [44] gives the concept of residual errors

$$\varepsilon_m^f = \frac{1}{k+1}\sum_{i=0}^{k}\left[N_f\left(\sum_{j=0}^{m} f(\zeta)\right)_{\eta=i\delta\eta}\right]^2, \quad (42)$$

$$\varepsilon_m^\theta = \frac{1}{k+1}\sum_{i=0}^{k}\left[N_\theta\left(\sum_{j=0}^{m} f(\zeta),\ \sum_{j=0}^{m}\theta(\zeta)\right)_{\eta=i\delta\eta}\right]^2, \quad (43)$$

$$\varepsilon_m^\phi = \frac{1}{k+1}\sum_{i=0}^{k}\left[N_\phi\left(\sum_{j=0}^{m} f(\zeta),\ \sum_{j=0}^{m} g(\zeta),\ \sum_{j=0}^{m}\phi(\zeta)\right)_{\eta=i\delta\eta}\right]^2, \quad (44)$$

The total squared residual error is given by [45]

$$\varepsilon_m^t = \varepsilon_m^f + \varepsilon_m^\theta + \varepsilon_m^\phi, \quad (45)$$

here, ε_m^t signifies a total squared residual error.

Figure 2 is drafted to analyze the total squared residual error. Computational results for an individual averaged squared residual error are demonstrated in Table 2.

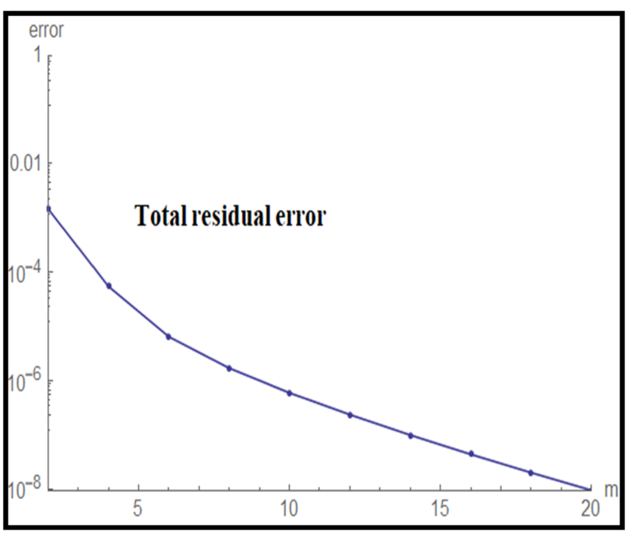

Figure 2: Total residual error.

Table 2: Numerical outcomes for individual averaged squared residual errors

m	ε_m^f	ε_m^θ	ε_m^ϕ
2	0.0000928964	0.000319415	0.000174965
4	4.09845×10^{-8}	8.06756×10^{-7}	8.02567×10^{-7}
8	1.01823×10^{-10}	4.68889×10^{-9}	1.07665×10^{-9}
10	1.40314×10^{-11}	1.21154×10^{-10}	1.00124×10^{-9}
14	1.66145×10^{-13}	5.69654×10^{-11}	2.72124×10^{-10}
18	2.07356×10^{-14}	9.94564×10^{-12}	3.87564×10^{-11}

Here, the obtained results indicate an excellent agreement.

3 Discussion

The physical impact of influential variables on the velocity field, entropy rate, thermal field, concentration, and Bejan number is scrutinized. The influence of flow variables on physical quantities is graphically studied.

3.1 Velocity

The The influence of velocity on the variation of the porosity variable is shown in Figure 3. A manifestation in the porosity variable augments the viscous force, which enhances resistance in the flow region. Thus, the velocity diminishes. The physical feature of the velocity against the Forchheimer number is examined in Figure 4. Here, the velocity decreases with a higher Forchheimer number. An increase in the magnetic variable rises the Lorentz force, which improves disturbance to liquid flow, and consequently, declines the velocity (Figure 5). Figure 6 presents the influence of the unsteadiness variable on velocity. One can find that velocity is the decaying function of (A).

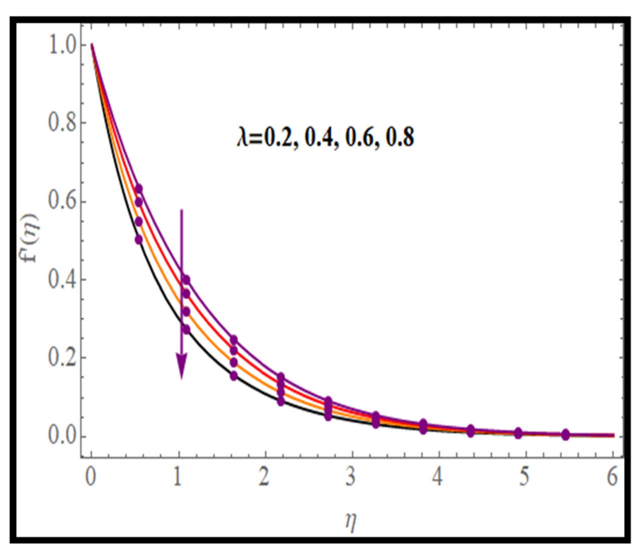

Figure 3: $f'(\eta)$ *via* λ.

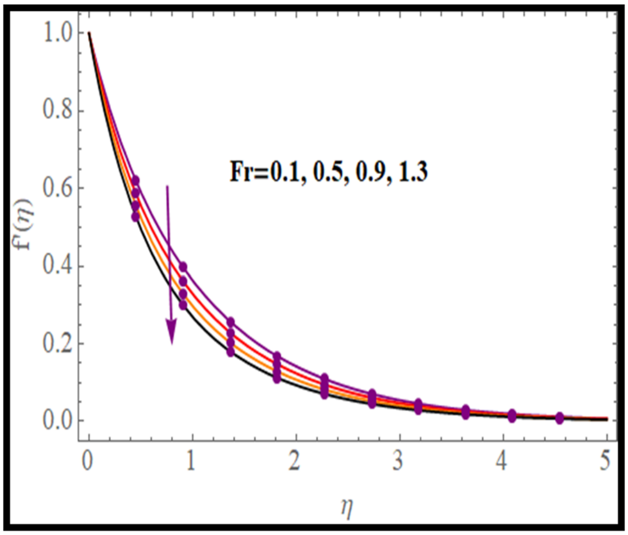

Figure 4: $f'(\eta)$ *via* Fr.

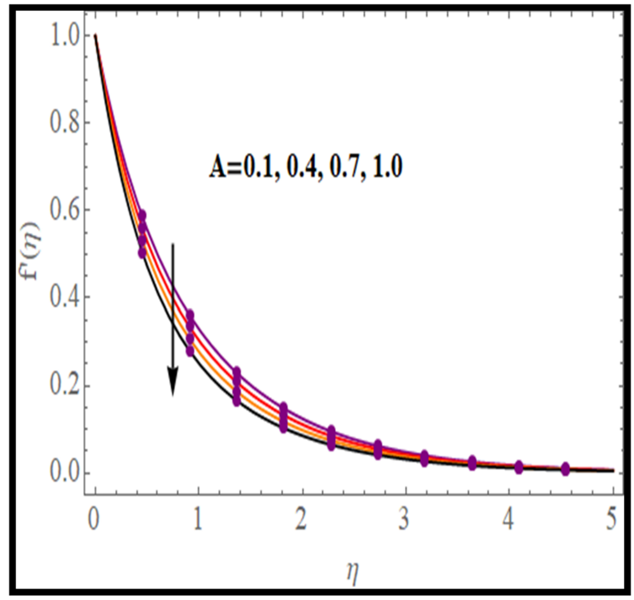

Figure 6: $f'(\eta)$ *via* A.

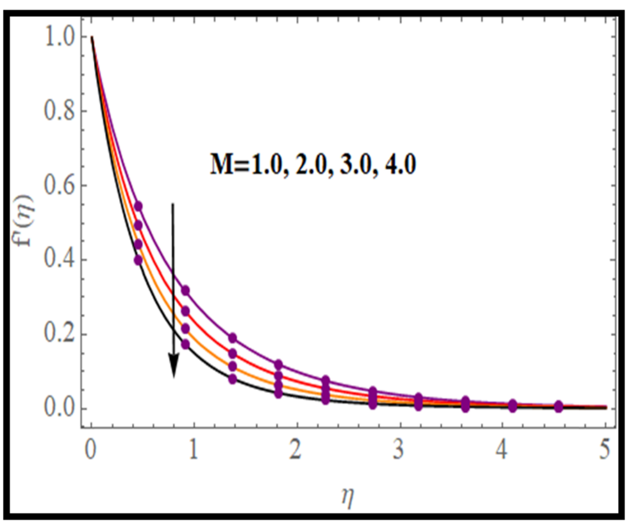

Figure 5: $f'(\eta)$ *via* M.

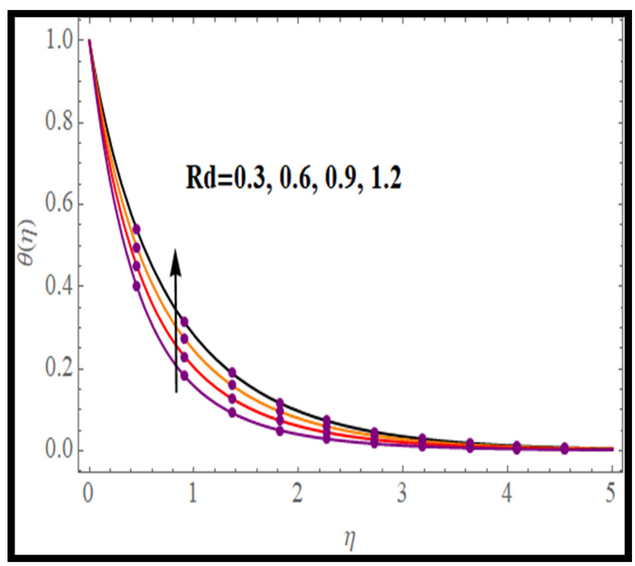

Figure 7: $\theta(\eta)$ *via* Rd.

3.2 Temperature

Prominent effects of influential variables like Rd, Du, M, and Ec on the thermal field are demonstrated in Figures 7–10. The impact of thermal field on radiation is portrayed in Figure 7. In fact, radiation is the combined effect of heat and thermal radiation transfer rates. Thus, an increase in radiation augments temperature. The prominent effect of M on the thermal field is drafted in Figure 8. Physically, an amplification in magnetic variable produces more resistance, which rises collision between liquid particles. Thus, an improvement in temperature is seen. A physical description of temperature *versus* Dufour number is disclosed in Figure 9. Clearly, temperature boosts up for a higher Dufour number. The thermal field performance against the Eckert number is shown in Figure 10. An increase in Eckert's number increases the kinetic energy, which enhances temperature.

3.3 Concentration

Variation of flow variables like Sc, γ, and Sr on concentration are displayed in Figures 11–13. The influence of

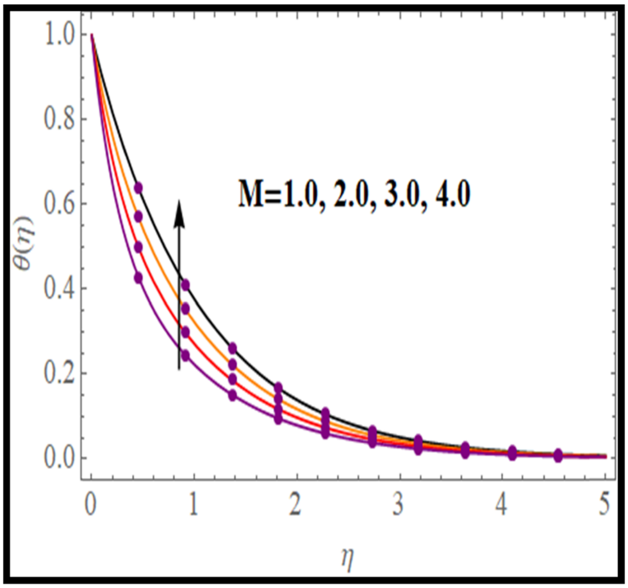

Figure 8: $\theta(\eta)$ *via* M.

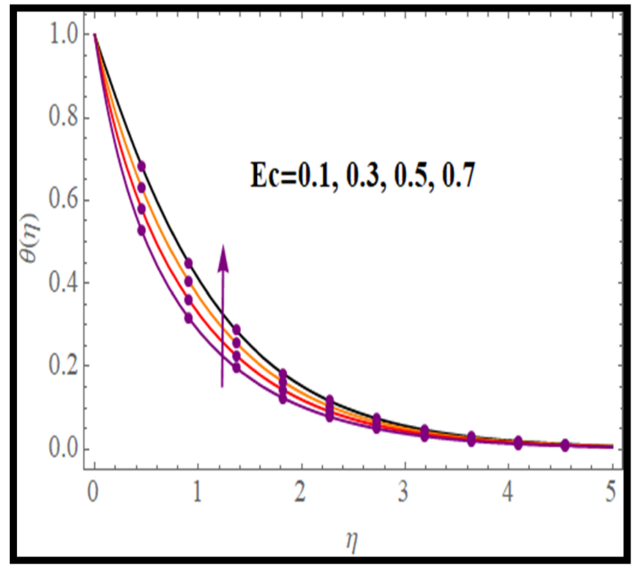

Figure 10: $\theta(\eta)$ *via* Ec.

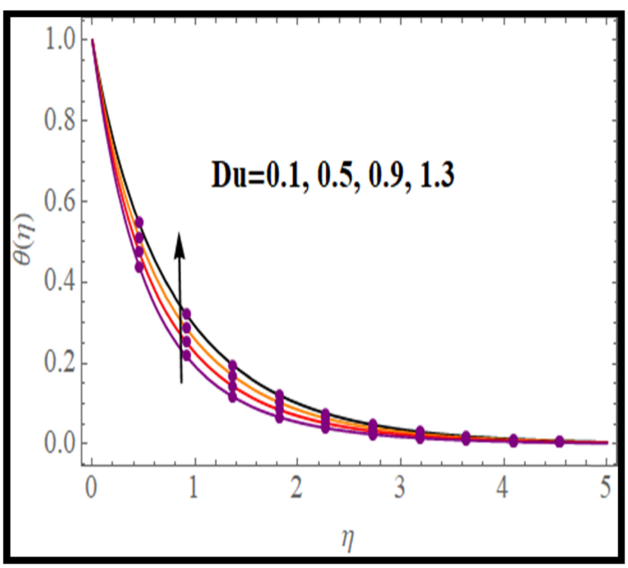

Figure 9: $\theta(\eta)$ *via* Du.

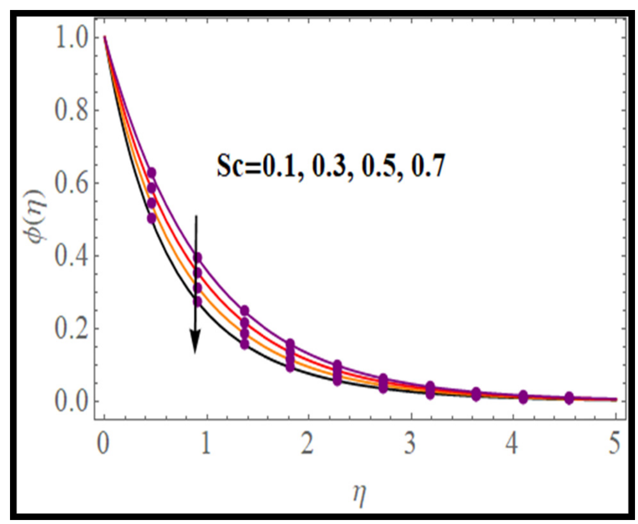

Figure 11: $\phi(\eta)$ *via* Sc.

the Schmidt number on $\phi(\eta)$ is shown in Figure 11. A reduction occurs in mass diffusivity with the Schmidt number, which declines the concentration. Higher approximation of reaction variables diminishes the concentration (Figure 12). The prominent variation in the concentration against the Soret number is disclosed in Figure 13. An increase in the Soret number corresponds to a decline in the concentration.

3.4 Entropy optimization and Bejan number

The influence of radiation on Be and N_G is shown in Figures 14 and 15. An intensification in both Bejan number and entropy rate is noticed with radiation. In fact, an increment in radiation increases the emission of radiation, which enhances disordering in the thermal system. Therefore, the entropy rate enhances. Figures 16 and 17 sketch the influence of the porosity variable on (Be) and (N_G). A reverse trend holds for the Bejan number and entropy rate

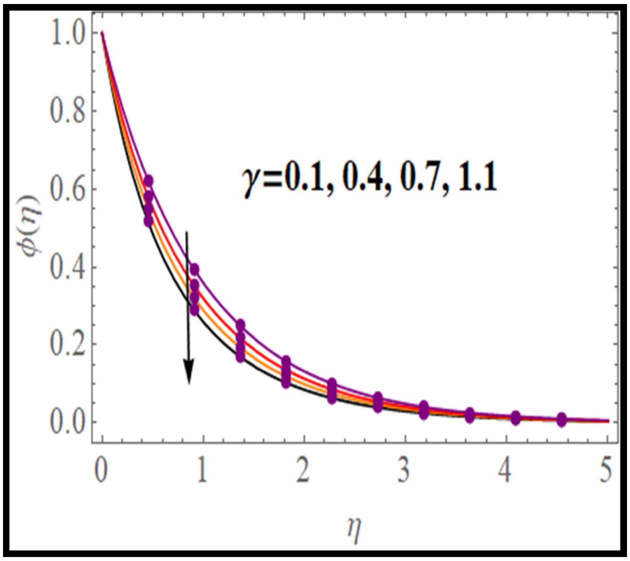

Figure 12: $\phi(\eta)$ *via* γ.

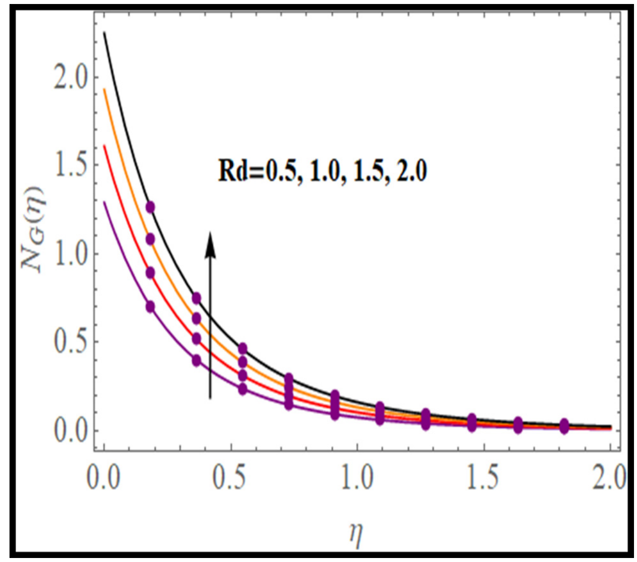

Figure 14: N_G *via* Rd.

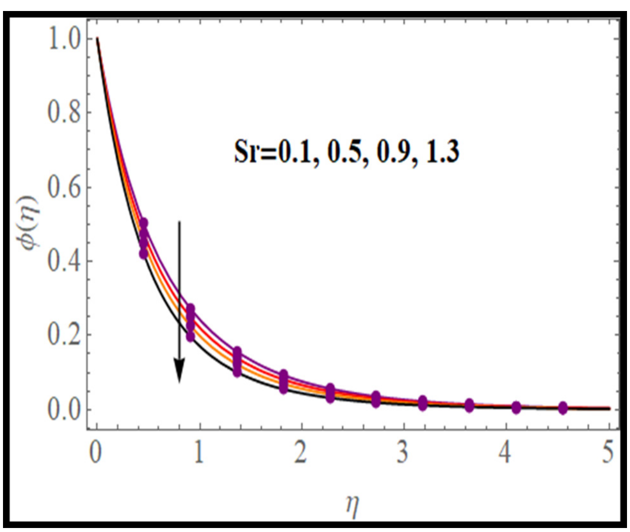

Figure 13: $\phi(\eta)$ *via* Sr.

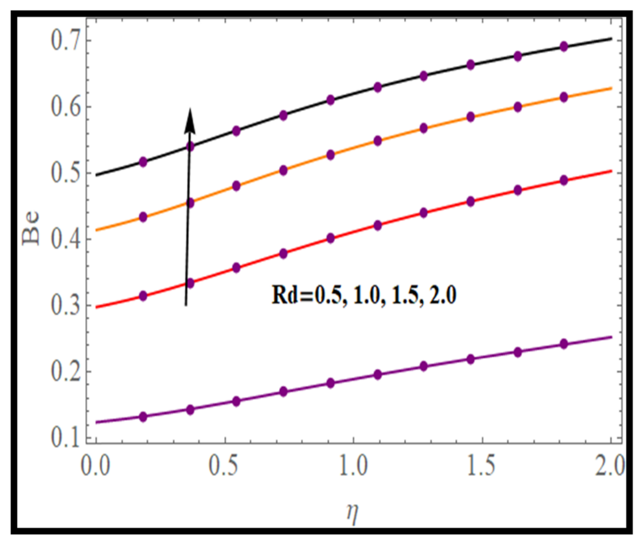

Figure 15: Be *via* Rd.

through the porosity variable. Figures 18 and 19 interpret the Brinkman number effect on Be and N_G. An opposite effect is noted for (Be) and (N_G) *versus* the Brinkman number. An increase in the Brinkman number increases viscous force, which improves collision between liquid particles. Thus, the entropy rate enhaces.

3.5 Physical quantities

The influence of sundry variables on drag force, gradient of temperature, and Sherwood number is studied.

3.5.1 Skin friction

The influence of porosity and magnetic variables on drag force is demonstrated in Figure 20. An increment in drag force is seen with variations in magnetic and porosity variables.

3.5.2 Nusselt number

Figures 21 and 22 elucidate the performance of the Nusselt number *via* involved variables. An increase in

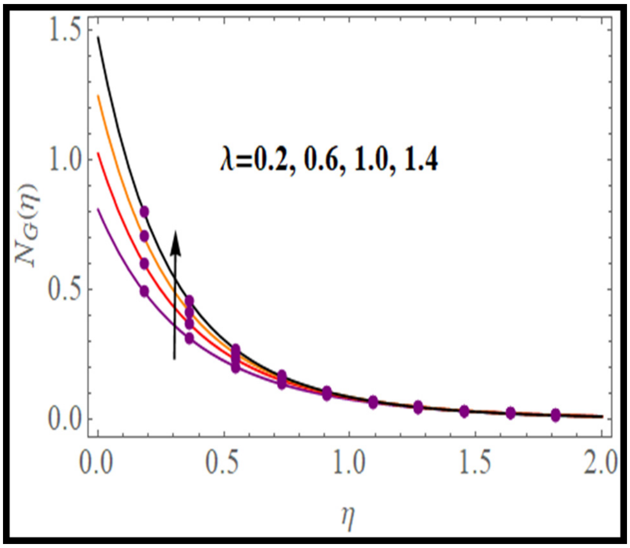

Figure 16: N_G *via* λ.

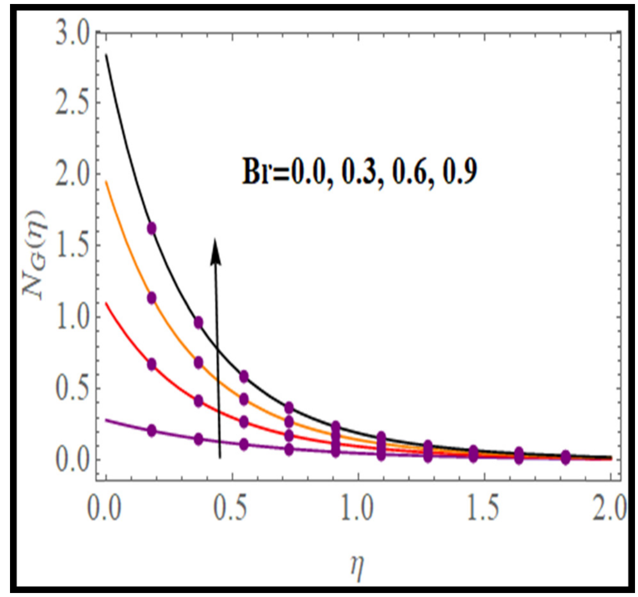

Figure 18: N_G *via* Br.

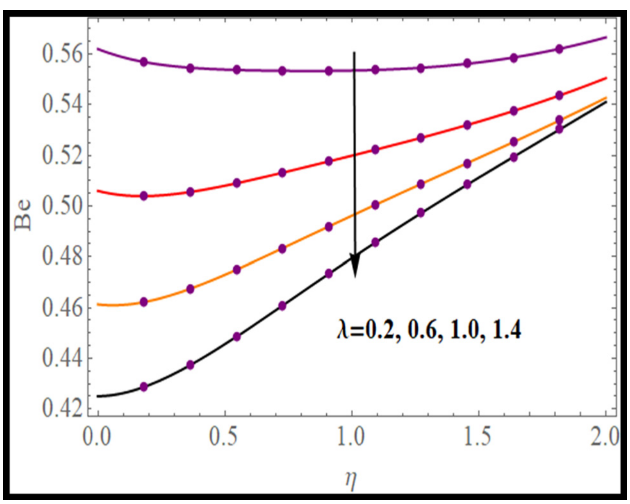

Figure 17: Be *via* λ.

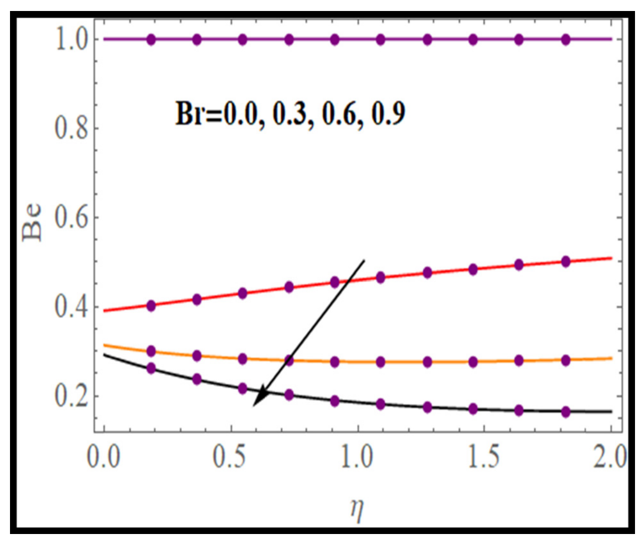

Figure 19: Be *via* Br.

heat transfer rate is observed under magnetic and radiation effects. A reverse trend holds for the temperature gradient with the Prandtl number and Brinkman numbers.

3.5.3 Sherwood number

Figure 23 shows the effect of Soret and Schmidt numbers on the Sherwood number. An improvement in the mass transfer rate is seen with Sr and Sc.

4 Conclusions

The main points of the present study are listed below:
- A reduction occurs in the velocity profile *via* unsteadiness and porosity variables.
- The velocity profile decreases with the Forchheimer number.
- An opposite effect on thermal field and velocity is noted through the magnetic variable.

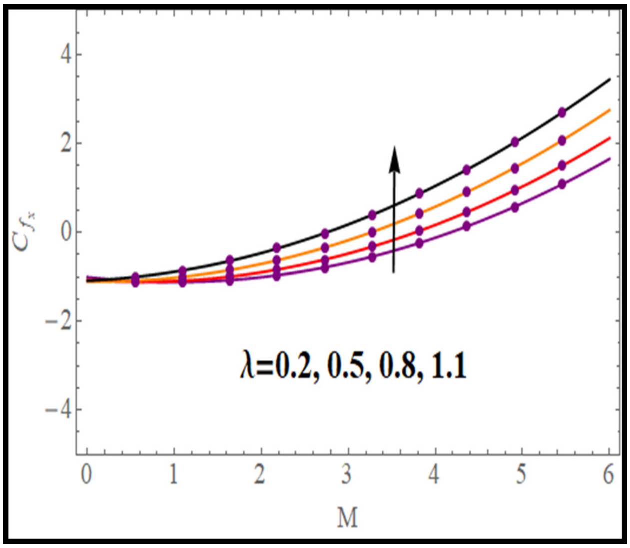

Figure 20: C_{fx} *via* M and λ.

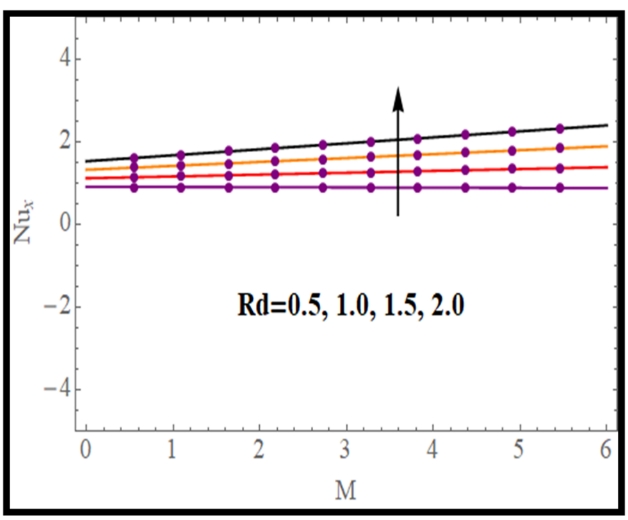

Figure 21: Nu_x *via* Rd and M.

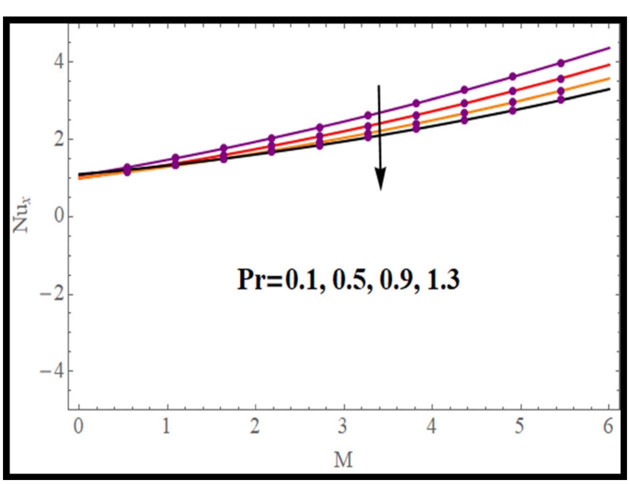

Figure 22: Nu_x *via* Br and Pr.

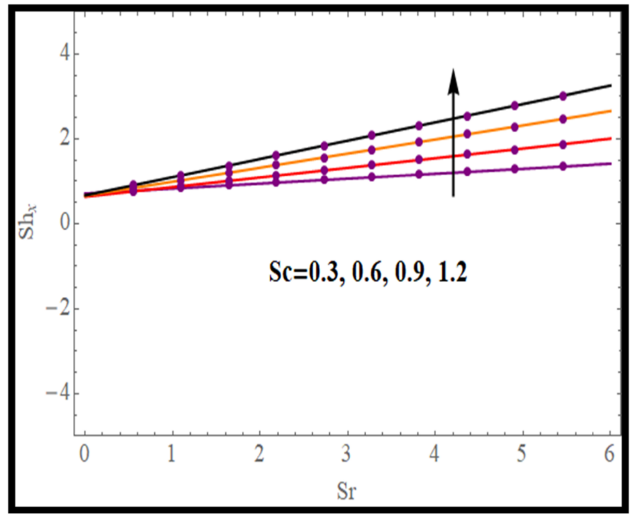

Figure 23: Sh_x *via* (Sr) and (Sc).

- An increase in the thermal field is seen through radiation.
- A higher Dufour number boosts up the thermal field.
- An increment in the Eckert number improves the thermal field.
- Concentration reduces with the Schmidt number.
- A reduction in the concentration occurs for reaction variables.
- An increase in the Soret number decreases the concentration.
- Higher radiation improves Bejan number.
- An augmentation in entropy rate is noticed through porosity variable.
- An opposite effect on the Bejan number and entropy rate is noted through the Brinkman number.
- An increase in drag force is noticed through magnetic variable.
- Higher radiation increases the heat transfer rate.
- Mass transfer rate increases with a higher Soret number.

Acknowledgments: The authors are grateful to Deanship of Scientific Research (DSR) at King Abdulaziz University (KAU), Jeddah, Saudi Arabia for funding this project, under grant no. (RG-4-130-43).

Funding information: The Deanship of Scientific Research (DSR) at King Abdulaziz University (KAU), Jeddah, Saudi Arabia has funded this project, under grant no. (RG-4-130-43).

Author contributions: All authors have accepted responsibility for the entire content of this manuscript and approved its submission.

Conflict of interest: The authors state no conflict of interest.

References

[1] Mahdy A. MHD non-Darcian free convection from a vertical wavy surface embedded in porous media in the presence of Soret and Dufour effect. Int Commun Heat Mass Tran. 2009;36:1067–74.

[2] Raveendra PH, Veena, Pravin VK. Mixed convective heat and mass transfer MHD flow past an unsteady stretching sheet with internal heat generation, viscous dissipation, internal mass diffusion including Soret and Dufour effects. Int J Advan Rese Eng Techno. 2017;8:17–33.

[3] Khan SA, Hayat T, Khan MI, Alsaedi A. Salient features of Dufour and Soret effect in radiative MHD flow of viscous fluid by a rotating cone with entropy generation. Int J Hydrogen Energy. 2020;45:14552–64.

[4] Reddy PS, Chamkha AJ. Soret and Dufour effects on unsteady MHD heat and mass transfer from a permeable stretching sheet with thermophoresis and non-uniform heat generation/absorption. J App Fluid Mech. 2016;9:2443–55.

[5] Hayat T, Nasir T, Khan MI, Alsaedi A. Numerical investigation of MHD flow with Soret and Dufour effect. Resul Phys. 2018;8:1017–102.

[6] Mahabaleshwar US, Nagaraju KR, Kumar PNV, Nadagoud MN, Bennacer R, Sheremet MA. Effects of Dufour and Soret mechanisms on MHD mixed convective-radiative non-Newtonian liquid flow and heat transfer over a porous sheet. Ther Sci Eng Prog. 2019;16:100459. doi: 10.1016/j.tsep.2019.100459.

[7] Kafoussias NG, Williams EW. Thermal-diffusion and diffusion-thermo effects on mixed free-forced convective and mass transfer boundary layer flow with temperature dependent viscosity. Int J Eng Sci. 1995;33:1369–84.

[8] Hayat T, Khan SA, Khan MI, Alsaedi A. Irreversibility characterization and investigation of mixed convective reactive flow over a rotating cone. Comp Meth Prog Biomed. 2020;185:105168. doi: 10.1016/j.cmpb.2019.105168.

[9] Mudhaf AFA, Rashad AM, Ahmed SE, Chamkha AJ, Kabeir SMME. Soret and Dufour effects on unsteady double diffusive natural convection in porous trapezoidal enclosures. Int J Mech Sci. 2018;140:172–8.

[10] Eldabe N, Zeid MA. Thermal diffusion and diffusion thermo effects on the viscous fluid flow with heat and mass transfer through porous medium over a shrinking sheet. J Appl Math. 2013;2013(2013):1–11. doi: 10.1155/2013/584534.

[11] Hayat T, Aslam N, Alsaedi A, Rafiq M. Numerical analysis for endoscope and Soret and Dufour effects on peristalsis of Prandtl fluid. Result Phys. 2017;7:2855–64.

[12] Cho QR, Chan CL. Numerical study of double-diffusive convection in a vertical cavity with Soret and Dufour effects by lattice Boltzmann method on GPU. Int J Heat Mass Tran. 2016;93:538–53.

[13] Hayat T, Ullah I, Muhammad T, Alsaedi A. Radiative three-dimensional flow with Soret and Dufour effects. Int J Mech Sci. 2017;133:829–37.

[14] Mahanthesh B, Mackolil J, Radhika M, Al-Kouz W, Siddabasappa. Significance of quadratic thermal radiation and quadratic convection on boundary layer two-phase flow of a dusty nanoliquid past a vertical plate. Int Communi Heat Mass Trans. 2021;120:105029. doi: 10.1016/j.icheatmasstransfer.2020.105029.

[15] Sulochana C, Samrat SP, Sandeep N. Boundary layer analysis of an incessant moving needle in MHD radiative nanofluid with joule heating. Int J Mech Sci. 2017;128:326–31.

[16] Thriveni K, Mahanthesh B. Significance of variable fluid properties on hybrid nanoliquid flow in a micro-annulus with quadratic convection and quadratic thermal radiation: Response surface methodology. Int Commun Heat Mass Trans. 2021;124:105264. doi: 10.1016/j.icheatmasstransfer.2021.105264.

[17] Hayat T, Tamoor M, Khan MI, Alsaedi A. Numerical simulation for nonlinear radiative flow by convective cylinder. Resul Phy. 2016;6:1031–5.

[18] Prakash J, Tripathi D. Electroosmotic flow of Williamson ionic nanoliquids in a tapered microfluidic channel in presence of thermal radiation and peristalsis. J Mol Liq. 2018;256:352–71.

[19] Mebarek-Oudina F, Bessaih R, Mahanthesh B, Chamkha AJ, Raza J. Magneto-thermal-convection stability in an inclined cylindrical annulus filled with a molten metal. Int J Numer Meth Heat Fluid Flow. 2020;31:1172–89. doi: 10.1108/HFF-05-2020-0321.

[20] Mehrez Z, Cafsi AE. Heat exchange enhancement of ferrofluid flow into rectangular channel in the presence of a magnetic field. Appl Math Comput. 2021;391:125634. doi: 10.1016/j.amc.2020.125634.

[21] Gholinia M, Hoseini ME, Gholinia S. A numerical investigation of free convection MHD flow of Walters-B nanofluid over an inclined stretching sheet under the impact of Joule heating. Therm Sci Eng Prog. 2019;11:272–82.

[22] Hayat T, Aslam N, Khan MI, Khan MI, Alsaedi A. Physical significance of heat generation/absorption and Soret effects on peristalsis flow of pseudoplastic fluid in an inclined channel. J Mol Liq. 2019;275:599–615.

[23] Reddy RCS, Reddy PS. A comparative analysis of unsteady and steady Buongiorno's Williamson nanoliquid flow over a wedge with slip effects. Chin J Chemi Eng. 2020;28:1767–77.

[24] Ramana Reddy JV, Sugunamma V, Sandeep N. Simultaneous impacts of Joule heating and variable heat source/sink on MHD 3D flow of Carreau-nanoliquids with temperature dependent viscosity. Nonlinear Eng. 2019;8:356–67.

[25] Mehrez Z, Cafsi AE. Thermodynamic analysis of Al_2O_3 – water nanofluid flow in an open cavity under pulsating inlet condition. Int J App Computat Math. 2017;3:489–510.

[26] Mehreza Z, Cafsi AE. Forced convection Fe_3O_4/water nanofluid flow through a horizontal channel under the influence of a non-uniform magnetic field. Eur Phys J Plus. 2021;136:451. doi: 10.1140/epjp/s13360-021-01410-2.

[27] Hayat T, Khan SA, Khan MI, Alsaedi A. Theoretical investigation of Ree – Eyring nanofluid flow with entropy optimization and Arrhenius activation energy between two rotating disks. Comp Method Progr Biomed. 2019;177:57–68.

[28] Farooq M, Javed M, Khan MI, Anjum A, Hayat T. Melting heat transfer and double stratification in stagnation flow of viscous nanofluid. Resul Phy. 2017;7:2296–301.

[29] Khan SA, Saeed T, Khan MI, Hayat T, Khan MI, Alsaedi A. Entropy optimized CNTs based Darcy–Forchheimer nanomaterial flow between two stretchable rotating disks. Int J Hydrogen Energy. 2019;44:31579–92.
[30] Khan SA, Hayat T, Alsaedi A. Entropy optimization in passive and active flow of liquid hydrogen based nanoliquid transport by a curved stretching sheet. Int Commun Heat Mass Trans. 2020;119:104890. doi: 10.1016/j.icheatmasstransfer.2020.104890.
[31] Bejan A. Second law analysis in heat transfer. Energy Int J. 1980;5:721–32.
[32] Bejan A. A study of entropy generation in fundamentsl convective heat transfer. ASME J Heat Tran. 1979;101:718–25.
[33] Khan SA, Hayat T, Alsaedi A, Ahmad B. Melting heat transportation in radiative flow of nanomaterials with irreversibility analysis. Renew Sustain Energy Rev. 2021;140:110739. doi: 10.1016/j.rser.2021.110739.
[34] Seth GS, Kumar R, Bhattacharyya A. Entropy generation of dissipative flow of carbon nanotubes in rotating frame with Darcy–Forchheimer porous medium: A numerical study. J Mol Liq. 2018;268:637–46.
[35] Kefayati GR. Simulation of double diffusive natural convection and entropy generation of power-law fluids in an inclined porous cavity with Soret and Dufour effects (Part II: Entropy generation). Int J Heat Mass Tran. 2016;94:582–624.
[36] Mehrez Z, Cafsi AE, Belghith A, Quéré PL. Effect of heated wall position on heat transfer and entropy generation of Cu – water nanofluid flow in an open cavity. Canadian J Phy. 2015;93:1615–29. doi: 10.1139/cjp-2014-0388.
[37] Mehrez Z, Cafsi AE, Belghith A, Quéré PL. MHD effects on heat transfer and entropy generation of nanofluid flow in an open cavity. J Magnet Magnet Mater. 2015;374:214–24.
[38] Mondal P, Mahapatra TR. MHD double-diffusive mixed convection and entropy generation of nanofluid in a trapezoidal cavity. Int J Mech Sci. 2021;208:106665. doi: 10.1016/j.ijmecsci.2021.106665.
[39] Qayyum S, Hayat T, Khan MI, Khan MI, Alsaedi A. Optimization of entropy generation and dissipative nonlinear radiative Von Karman's swirling flow with Soret and Dufour effects. J Mol Liq. 2018;262:261–74.
[40] Yousofvand R, Derakhshan S, Ghasemi K, Siavashi M. MHD transverse mixed convection and entropy generation study of electromagnetic pump including a nanofluid using 3D LBM simulation. Int J Mech Sci. 2017;133:73–90.
[41] Mliki B, Abbassi MA. Entropy generation of MHD natural convection heat transfer in a heated incinerator using hybrid-nanoliquid. Propul Power Res. 2021;10:143–54.
[42] Khan MI, Qayyum S, Hayat T, Khan MI, Alsaedi A. Entropy optimization in flow of Williamson nanofluid in the presence of chemical reaction and Joule heating. Int J Heat Mass Trans. 2019;133:959–67.
[43] Marzougui S, Mebarek-Oudina F, Aissa A, Magherbi M, Shah Z, Ramesh K. Entropy generation on magneto-convective flow of copper-water nanofluid in a cavity with chamfers. J Ther Anal Calori. 2020;143:2203–14. doi: 10.1007/s10973-020-09662-3.
[44] Liao SJ. An optimal homotopy-analysis approach for strongly nonlinear differential equations. Commun Nonlinear Sci Numer Simul. 2010;15:2003–16.
[45] Hayat T, Khan SA, Khan MI, Alsaedi A. Optimizing the theoretical analysis of entropy generation in the flow of second grade nanofluid. Phy Scripta. 2019;94:085001. doi: 10.1088/1402-4896/ab0f65.
[46] Wang CY. Free convection on a vertical stretching surface. J Appl Math Mech (ZAMM). 1989;69:418–20.
[47] Gorla RSR, Sidawi I. Free convection on a vertical stretching surface with suction and blowing. Appl Sci Res. 1994;52:247–57.